Int. J. Electrochem. Sci., 14 **(2019)** 1855 – 1868, doi: 10.20964/2019.02.12

International Journal of
ELECTROCHEMICAL
SCIENCE
www.electrochemsci.org

Performance of Coating Based on β-CD-g-GO/epoxy Composites for the Corrosion Protection of Steel

Chun Feng [1,2,], Lijuan Zhu[1,2], Yaqiong Cao[1,2],Yin Di[3], Zongxue Yu[3,*], Guhui Gao[4]*

[1] CNPC Tubular goods research institute, Xi'an, 710077, China.
[2] State Key Laboratory for Performance and Structure Safety of Petroleum Tubular Goods and Equipment Materials, Xi'an, 710077, China.
[3] Southwest Petroleum University, School of Chemistry and Chemical Engineering, Chengdu, 610500, China.
[4] Redbud Innovation Institute, Baodi, Tianjin,301800, China.
[*]E-mail: fengchun003@cnpc.com.cn haiqingy@163.com

Received: 27 July 2018 / *Accepted:* 21 September 2018 / *Published:* 5 January 2019

This study reports a new strategy for enhancing the anti-corrosion properties of epoxy coatings. For this purpose, beta-cyclodextrin-graphene oxide (β-CD-g-GO) nanosheets were synthesized via anchoring beta-cyclodextrin on a graphene oxide surface in the presence of 3-glycidoxypropyltrimethoxysilane (KH560). The structure of the material was characterized by SEM, EDX, XRD, FT-IR and TGA. The inclusion of 2 wt. % GO and β-CD-g-GO nanosheets in epoxy resin remarkably enhanced the corrosion protection performance of the material relative to that of pure epoxy coating. Electrochemical impedance spectroscopy (EIS) measurements revealed that the impedance of the epoxy coating was improved after the addition of 2 wt. % GO and β-CD-g-GO nanosheets. The most pronounced improvement in the properties of the epoxy coating was obtained using β-CD-g-GO nanosheets. Scratches tests confirmed the reduced steel substrate corrosion in the case of epoxy coating that included β-CD-g-GO nanosheets compared to the corrosion obtained for other samples.

Keywords: Graphene oxide, Beta-cyclodextrin, Corrosion resistance, Epoxy coating

1. INTRODUCTION

With the development of oilfield entering the high water-cut stage, the damage of the water injection string is becoming increasingly serious. Conventional anticorrosion technology of the water injection string, such as organic coatings, have inevitable pin holes and show poor wear and erosion resistance. This brings a hidden danger for safety of production and environment of oil fields. Organic coatings are the most popular and effective coating used to control or mitigate the corrosion processes that take place on steel surfaces exposed to severe environments[1, 2]. The organic coatings protect the

steel from corrosion through barrier mechanisms associated with coatings [3, 4]. Among organic coatings, epoxy coatings are frequently used owing to their excellent adhesion properties, low shrinkage and price, outstanding chemical stability and corrosion resistance [5-7]. However, epoxy coatings produce a multitude of cracks in the curing process that are permeable to corrosive electrolytes, which leads to the formation of corrosion products beneath the coating. Therefore, epoxy coatings cannot provide long-term corrosion protection[8, 9]. To enhance the anti-corrosion performance of epoxy coating, adding nanomaterials into the epoxy coating is an excellent strategy [10-12].

Graphene oxide (GO) is a two-dimensional (2D) sheet-structure nanomaterial. The application of GO for the protection of metallic substrates from corrosion has been reported [13-17], as the sheet structure of GO can enhance the barrier mechanisms of epoxy coatings. However, GO has a pronounced tendency to aggregate due to high surface area and strong van der Waals forces of the material. This tendency leads GO to disperse poorly in epoxy resin[18, 19]. To improve the dispersibility of GO in epoxy resin and to improve the antiseptic properties of epoxy coatings including GO, the functionalization of GO has been an effective approach, owing to the many functional groups, including hydroxyl, carbonyl, carboxyl and epoxide groups, on the edges and basal planes of GO nanosheets [14, 20-22]. For instance, Zheng et al.[22] developed a new type of modified GO coating that retained the high dispersion of modified GO sheets in a polymer matrix; the results revealed that the modified GO sheets significantly reinforced the corrosion protection properties of epoxy coatings on a carbon steel substrate. Ahmadi et al.[14] prepared silylated graphene oxide through a sol–gel route, and the material could excellently disperse in a silane coating. The coating containing silanized graphene oxide showed superior corrosion-protection performance compared to unfilled silane coating, as determined by in electrochemical impedance spectroscopy (EIS).

β-CD is a natural macrocyclic polymers of glucose with the unique properties of external hydrophilicity and interior hydrophobicity[23, 24]. In addition, β-CD is widely used as a biomimetic systems and as a novel medium for chemical, photophysical, and photochemical studies[25]. The surface of β-CD contains hydroxyl groups, which are suitable reactive sites for modifying GO. In addition, one study [26] indicated that the dispersibility of GO was excellent upon the addition of β-CD.

In this study, the influence of a β-CD-g-GO material on the corrosion protection performance of epoxy coating was studied. First the β-CD-g-GO material was synthesized via anchoring β-CD on the GO surface with the help of KH560. After characterization of β-CD-g-GO by FT-IR, XRD, TGA and SEM analysis, 2 wt% β-CD-g-GO material was incorporated into the epoxy coating to prepare the β-CD-g-GO/epoxy coating. In addition, the corrosion protection performance of the β-CD-g-GO/epoxy samples was examined by EIS and scratch tests. Finally, the β-CD-g-GO material could excellently disperse in the epoxy coating, and the β-CD-g-GO/epoxy samples had far better anti-corrosion performance than did pure epoxy coating.

2. EXPERIMENTAL

2.1. Reagents

Natural graphite powder was obtained from Aladdin. Acetone, KH560, NaOH, DMF, β-CD, H_2SO_4, $KMnO_4$, $NaNO_3$, H_2O_2, HCl, and NaCl were purchased from Kelong Chemical Co. Ltd.,

Chengdu, China. The epoxy emulsion (WSP-6101) and its hardener were supplied by the Bluestar Technology Wuxi Resin Factory. Deionized water was produced by a water purification machine (UPCIII-40 L, Ulupure).

2.2. Synthesis of KH560/β-CD and β-CD-g-GO nanosheet

GO was synthesized by modified Hummers method[18, 27] from graphite. The synthesis route and mechanism of KH560/β-CD preparation is shown in Fig. 1. A minture of 5 g β-CD, 50 ml DMF, 10 ml KH560 and 0.1 g NaOH was stirred at 55 ℃ for 48 h under a nitrogen atmosphere. Then, moderate acetone was added, the resulting mixture was washed with acetone to remove excessive KH560, and the mixture was then dried in a vacuum at 40 ℃ to a constant weight.

KH560/β-CD (5.0 g) was adequately dissolved in 30 ml deionized water, and the pH of the mixed solution was adjusted by acetic acid solution (pH = 4~6). The solution was stirred for 1 h to obtain the hydrolytic product. Subsequently, GO (0.5 g) was dispersed in the mixture by ultrasonication for 0.5 h, and then the mixture was stirred at 85 ℃ for 10 h. The resulting solution was washed with deionized water repeatedly to obtain β-CD-g-GO nanosheets (Fig. 2).

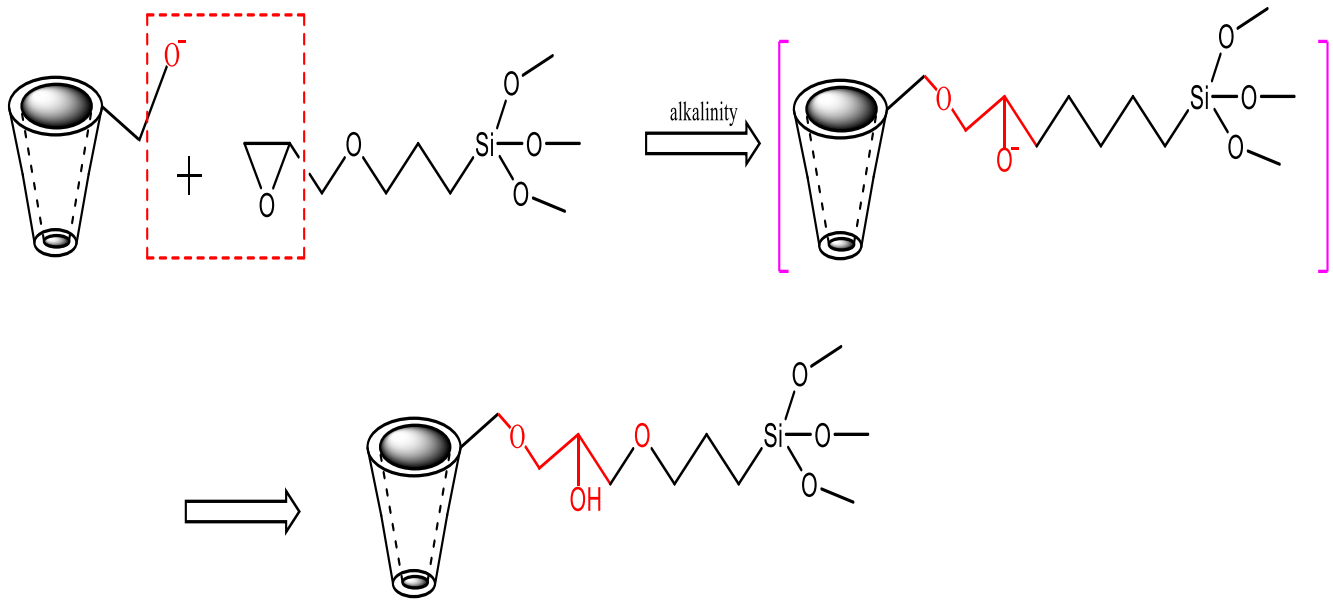

Figure 1. Diagram of the reaction mechanism of KH560/β-CD

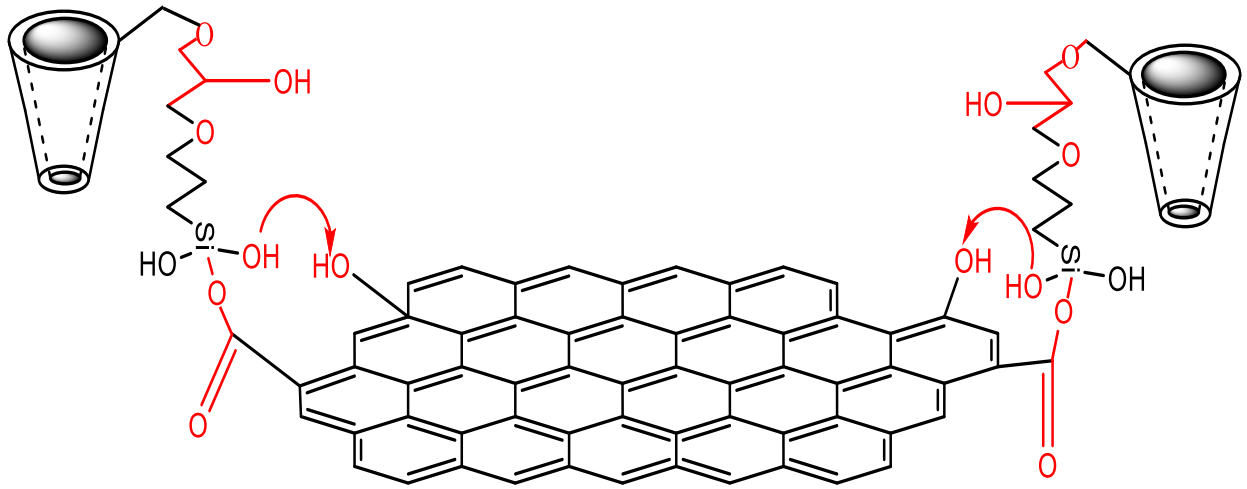

Figure 2. Diagram of the reaction mechanism of β-CD-g-GO nanosheets

2.3. Surface treatment of β-CD-g-GO/epoxy coating

β-CD-g-GO/epoxy coatings were prepared by adding β-CD-g-GO (2 wt.%) to the epoxy resin under ultrasonic oscillation and spraying the modified resin on the clean surface of steel sheets (10 × 10 mm). The mixture was hardened by applying the following series of temperatures and times: 60 °C for 1 h, 120 °C for 1 h, 180 °C for 0.5 h, and 220 °C for 1.5 h. Other coatings were also prepared through a similar process.

2.4. Characterization

The structure of all materials (H560, β-CD, KH560/β-CD and β-CD-g-GO) was characterized by Fourier transform infrared spectroscopy (FT-IR), X-ray diffraction (XRD, Holland), scanning electron microscopy (SEM, JSM-7500F) and thermo gravimetric analysis (TGA). SEM analysis was performed on a JSM-7500F instrument, (JEOL, Tokyo, Japan). FT-IR spectra of the samples were obtained from a WQF-520 instrument in the wavenumber range 4000–400 cm^{-1}. XRD analysis was conducted on a PANalytical instrument with a Cu Kα radiation source at a scan rate of 2° min^{-1} ranging from 5° to 70° (2θ). TGA (STA449F3) date were obtained from 30 to 800 °C with a heating rate of 5 °C min^{-1} under an air atmosphere.

The corrosion resistance of coatings was tested by an electrochemical workstation (EIS, CHI604D, China) in 3.5 wt. % NaCl solution. The analysis was carried out at room temperature with a three-electrode cell including a saturated calomel electrode (reference electrode), platinum plate electrode (counter electrode) and steel substrates without and with treatments (working electrode with an area of 1 cm^2). Measurement were performed at an open circuit potential (OCP) in the frequency range of 10^5 to 10^{-2} Hz with an amplitude sinusoidal voltage of ± 10 mV at different immersion times.

To investigate the anticorrosion ability of coatings, the scratch test is a common method. Therefore, scratches with 15 mm length and 2 mm width were created on the surface of coatings by a sharp scalpel. To make scratches with the same depth and width in all samples, the scratches were created

under a constant force on the surfaces of all samples. Then, the scratched substrates were immersed in 3.5 wt. % NaCl solution. Subsequently, optical photography was used to observe the amount of corrosion products.

3. RESULTS AND DISCUSSION

3.1. Structure analysis of the material

FT-IR spectra of KH560, β-CD, KH560/β-CD and β-CD-g-GO are shown in Fig. 3. The characteristic stretching vibration peaks of KH560 (Fig. 3a) were observed at 2942 cm^{-1} ($–CH_3$), 2836 cm^{-1} ($–CH_2–$) and, 1092 cm^{-1} (Si-O-Si). For β-CD (Fig. 3b), the characteristic peaks were at 3407 cm^{-1} (–OH) and 2930 cm^{-1} ($–CH_3$). For KH560/β-CD (Fig. 3c), the peak at approximately 2849 cm^{-1} was related to –CH2– and was seen in the spectra of KH560, but not those of β-CD. This result indicated that the β-CD had been successfully modified by KH560. Moreover, Fig. 3d shows the FT-IR spectra of the β-CD-g-GO hybrid material. The appearance of a new band at 1719 cm^{-1} was attributed to the C=O bond of GO[28]. The peaks at 2928 cm^{-1} and 1161 cm^{-1} corresponded to the stretching vibrations of the –CH2 and –C–O–C groups of β-CD, respectively. Additionally, the peak at 1085 cm^{-1} was associated with the stretching vibrations of the Si-O group of KH560. These results indicated that the KH560/β-CD was grafted on the surface of GO to some degree.

Some studies[29] have proved that if two materials are physically mixed, both characteristic peaks will appear in the diffraction spectrum. On the other hand, KH560 is liquid, so there is no diffraction spectrum. Fig. 4 shows the XRD patterns of β-CD, KH560/β-CD, GO and β-CD-g-GO. The original β-CD was a highly crystalline material with main diffractions peaks at 6.19º, 9.41º, 12.76º, 17.12º and 21.09º (2θ). By comparison, KH560/β-CD (Fig. 4b) presented a larger amorphous phase but had some intense crystalline traces, and only parts of the β-CD diffraction peaks were visible (2θ=6.12º, 12.71º, 17.17º). As discussed previously, if KH560 and β-CD were mixed physically, KH560/β-CD would display all the diffractions peaks of β-CD. In other words, KH560 reacted with β-CD, which was supported by the results of FT-IR analysis.

For GO (Fig. 4c), the characteristic diffraction peak appeared around at 2θ=10.03°, which was due to the embedding of a large number of oxygen-containing functional groups in the interlayer spacing of graphite[30, 31]. The diffraction peaks at 6.12º, 10.33º and 17.46º stemmed from the β-CD-g-GO material. Moreover, the characteristic diffraction peak of GO was still present, but the 2θ angle of the peaks of GO changed from 10.03º to 10.33º. Thus, the surface of GO was modified by KH560/β-CD.

The TG curves of KH560/β-CD, β-CD, GO and β-CD-g-GO are shown in Fig. 5. At 0~100 °C, the weight loss was primarily due to the loss of H_2O molecules that were physically adsorbed on the surface of samples. For β-CD, there was a main weight loss at approximately 300℃(68wt%), which was mainly due to the thermal decomposition of β-CD [32]. The weight loss of KH560/β-CD at 240℃ ~ 420℃ was due to the thermal decomposition of β-CD, and the weight loss was 59.75 wt.%. The loss trend of GO was consistent with the results of other research[33]; the weight loss observed at 110~310 °C was attributed to the decomposition of oxygen-containing functional groups that were present on the

basal plane of the GO nanosheets and corresponded to a value of approximately 24.83 wt.%. The weight-loss tendency of the β-CD-g-GO hybrid material was similar to those of KH560/β-CD and GO, while some differences still existed: (I) at approximately 190 ℃~310 ℃, the weight loss of the β-CD-g-GO hybrid was attributed to the decomposition of groups and crystal water that were present on the surface of the β-CD-g-GO hybrids material. (Π) At 310 ℃~ 550 ℃, the weight loss was due to decomposition of the carbon skeleton of β-CD-g-GO. Thus, TGA analysis also illustrated that the β-CD-g-GO hybrids was prepared successfully.

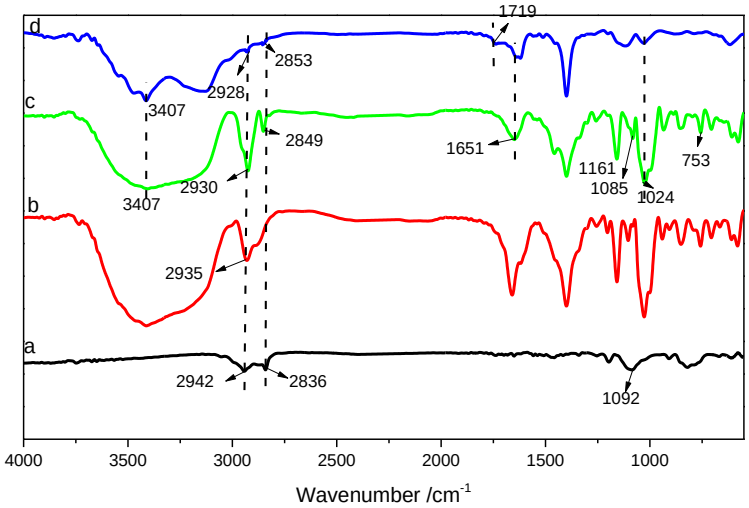

Figure 3. FTIR spectra of KH560 (a), β-CD (b), KH560/β-CD (c) and β-CD-g-GO (d)

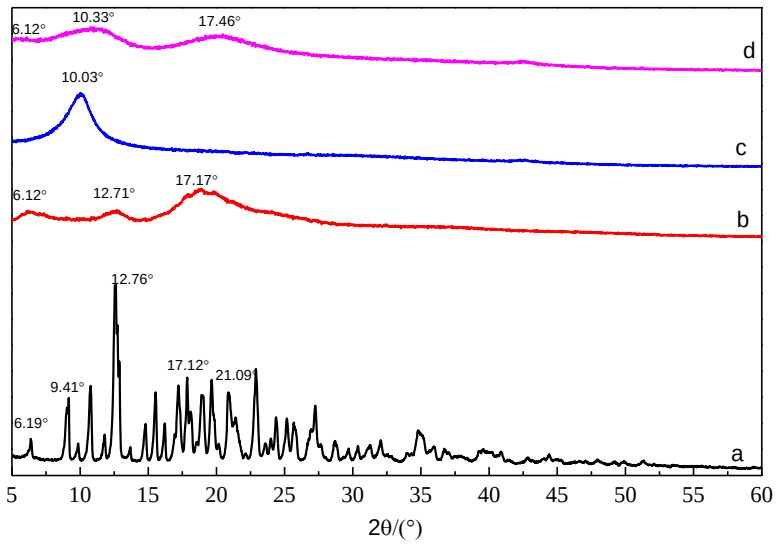

Figure 4. XRD spectra of β-CD (a), KH560/β-CD (b), GO (c) and β-CD-g-GO

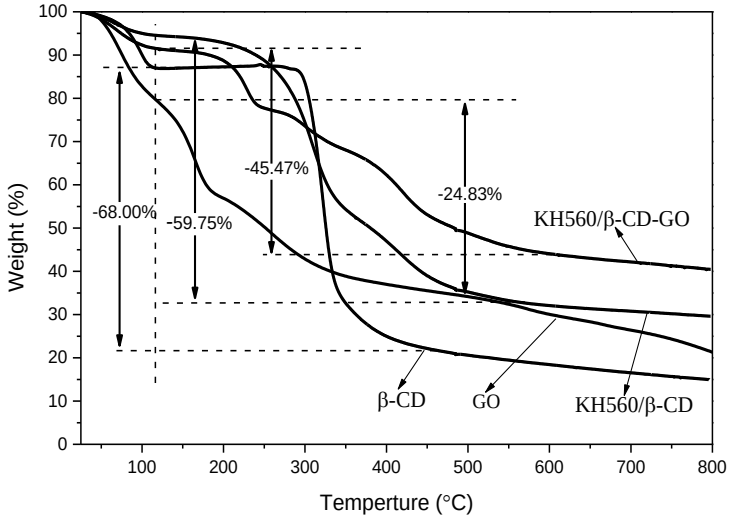

Figure 5. Thermo gravimetric (TGA) curves of β-CD, KH560/β-CD, GO and β-CD-g-GO

The morphologies and microstructures of GO, β-CD, KH560/β-CD and β-CD-g-GO were studied using SEM (Fig. 6). For the GO (Fig. 7a), the material had a typical sheet structure and some overlapping, which was attributed to the existence of various oxygen-containing groups on the surface of the GO[34, 35]. The structure of pure β-CD consisted of smooth rectangular blocks (Fig. 6b). The surface of β-CD was covered by a layer of organic matter (Fig. 6c), indicating that the β-CD had been modified by KH560 successfully. This was consistent with the results of FT-IR, XRD and TGA. The KH560/β-CD material was clearly observed on the GO sheet and had a wrinkled morphology, as marked with black ovals, in Fig. 6d. Thus, β-CD-g-GO sheets were fabricated successfully.

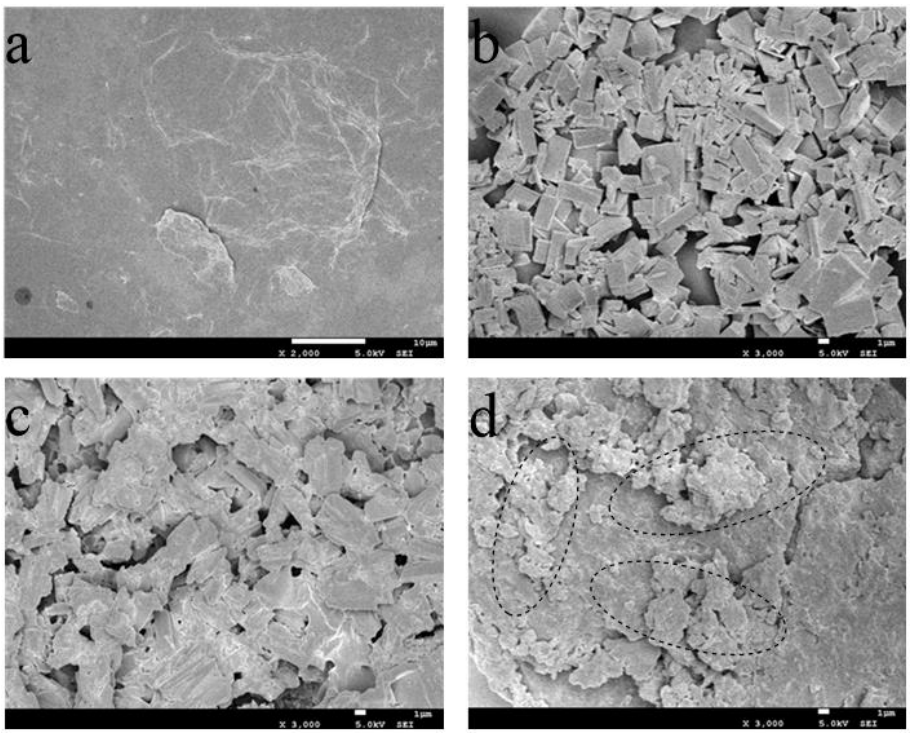

Figure 6. SEM images of GO (a), β-CD (b), KH560/β-CD (c) and β-CD-g-GO (d)

3.2. Dispersion of the β-CD-g-GO hybrid material in epoxy coatings

To evaluate the dispersion of GO and the β-CD-g-GO hybrid material in the matrix, the fracture morphology (SEM) is shown in Fig. 7. The pure epoxy (Fig. 7a) showed an extremely smooth and clean fracture surface. The dispersity of GO (Fig. 7b) was underdeveloped, which was due to the self-agglomeration of GO. However, the β-CD-g-GO (Fig. 7c) material had a better dispersion performance in epoxy resin. These results indicated that β-CD-g-GO could disperse in epoxy very well.

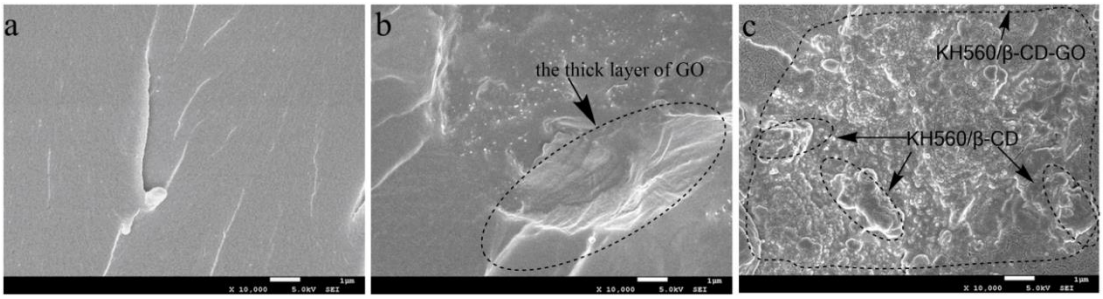

Figure 7. Fracture morphology of pure epoxy (a), GO/epoxy (b) and β-CD-g-GO/epoxy (c)

The XRD spectra of pure epoxy and β-CD-g-GO/epoxy are shown in Fig. 8. The neat epoxy had a wide diffraction range from 10 ° to 30 ° in the XRD spectra due to the amorphous structure of the cured epoxy molecules[36, 37]. However, the patterns of β-CD-g-GO/epoxy were similar to the diffraction patterns of the neat epoxy and lacked the peaks of the β-CD-g-GO hybrid material, which indicated that the β-CD-g-GO achieved proper dispersion in the EP matrix to some extent. The results were in agreement with SEM analysis.

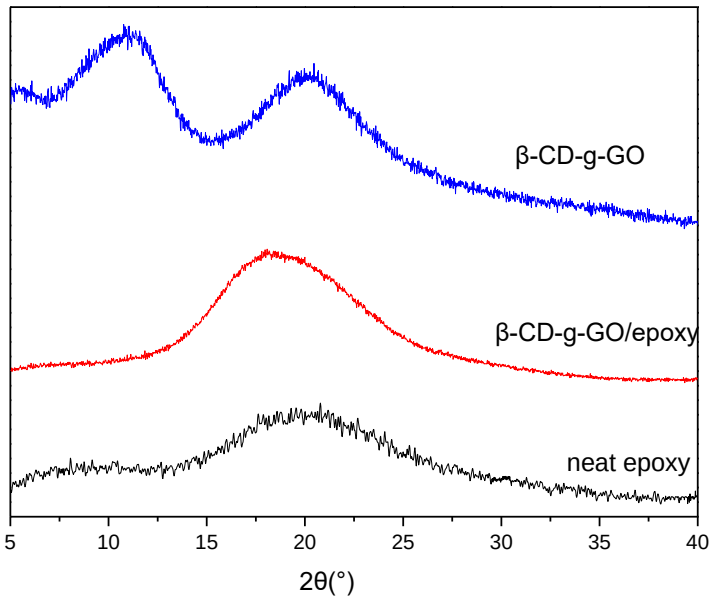

Figure 8. XRD spectra of β-CD-g-GO, pure epoxy and β-CD-g-GO/epoxy

3.3. Thermal stability of the β-CD-g-GO epoxy coating

Fig. 9 shows the thermo gravimetric analysis (TGA) and DTG curves of the pure epoxy coating, KH560/β-CD/epoxy coating and β-CD-g-GO /epoxy composite coating. All coatings had no obvious weight loss before 350 ℃. After 350 ℃, all coatings had weight loss to different degrees, and the data are shown in table. 1. The KH560/β-CD/epoxy composite coating presented an evident weight loss at 350~800 ℃, which was due to the decomposition of the groups of KH560/β-CD and the corresponding DTG temperature was 409 ℃. However, pure epoxy, GO/epoxy and the β-CD-g-GO/epoxy composite coating corresponded to DTG temperatures of 422 ℃, 423 ℃ and 435 ℃, respectively. Moreover, the DTG data analysis revealed that the β-CD-g-GO/epoxy composite coating showed superior thermal stability relative to those of other coatings.

Table 1. Weight loss at different temperatures

Weight Loss	350℃	450℃	500℃	600℃	800℃
β-CD-g-GO/epoxy	1.853%	41.154%	60.267%	70.019%	69.537%
KH560/β-CD/epoxy	3.248%	54.513%	69.817%	75.458%	75.429%
GO/epoxy	3.118%	49.615%	59.069%	65.726%	69.041%
Pure epoxy	1.653%	48.030%	56.470%	62.411%	67.208%

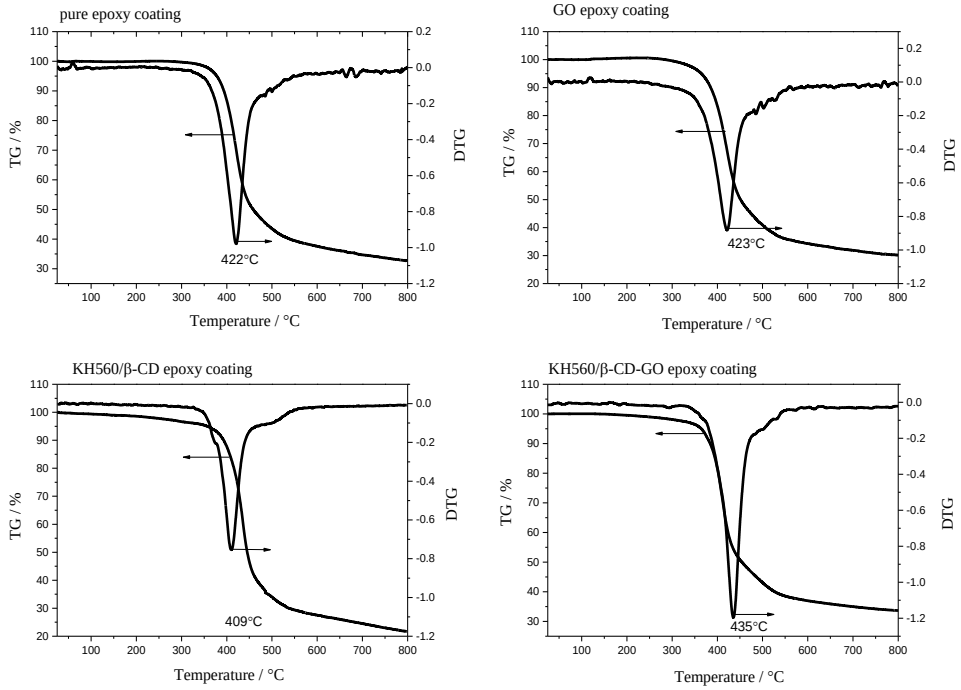

Figure 9. TG and DTG curves of pure epoxy coating (a), GO/epoxy coating (b), KH560/β-CD/epoxy coating (c) and β-CD-g-GO/epoxy coating (d)

3.4. Corrosion resistance analysis

The electrochemical impedance technique (EIS) was employed to evaluate the corrosion resistance of the coatings in 3.5wt% NaCl solution. The degree of corrosion was determined by fitting the EIS data to equivalent electric circuits reported in previous studies[38-40], and the results are shown in Fig. 10. The parameters included electrolyte resistance (Rs), coating capacitance (CPE_f), coating resistance (R_f), charge transfer resistance (Rct), double layer capacitance (CPE_{dl}) and Warburg impedance (W). In the initial stage (corresponding to Fig. 10a), the composite coating was equivalent to an isolation layer with high resistance and small capacitance. The capacitance of the coating increased and the resistance decreased with increased immersion time, and electrolytes solution did not penetrate into the interface between the coating and metal substrate. Then, with increased immersion time, NaCl solution penetrated the coating to the steel surface, and electro-chemical reactions occurred on the coating/metal interface. Therefore, Warburg impedance (corresponding to Fig. 10b) began to appear and the coating did not protect the metal.

Meanwhile, the coating resistance Rc and charge transfer resistance Rct are two important parameters to evaluate the protective performance for metals. And the fitting results of the equivalent electrical circuits after 2h immersion shown in table 2. The coating resistance Rc can reflect the defects and degradation degree of coatings. With the degradation of the coating, more defects will form and will result in the lower value of coating resistance. In addition, the charge transfer resistance (Rct) directly relates to the rate of the corrosion process at the electrolyte/metal interface. The higher the Rct is, the lower the corrosion rate is. Thus, compared with pure epoxy, β-CD-g-GO/epoxy composite coating exhibited a significant corrosion resistance property.

The EIS spectra of pure epoxy coating is shown in Fig. 11. The impedance of the pure epoxy coating obviously decreased with prolonged immersion time, which was due to the diffusion of some molecules (H_2O, O_2 and Cl^-) into the epoxy coating. The epoxy coating began to display clearly evident Warburg impedance at 96 h, and therefore could not protect the metal substrate after 96 h.

The impedance of the β-CD-g-GO/epoxy composite coating (Fig. 11) gradually decreased substantially. This trend was consistent with the corrosion process of pure epoxy coating, and Warburg impedance began to emerge at 264 h. However, the impedance value at 24 h was greater than at 36 h, and a similar situation emerged upon further immersion, which was due to the presence of β-CD.

In contrast with pure epoxy coating, the β-CD-g-GO/epoxy composite coating protected the metal substrate for a longer time from the electrochemical solution. Consequently, the pure epoxy coating and the β-CD-g-GO/epoxy composite coating could protect the metal substrate, and the corrosion resistance property of the β-CD-g-GO/epoxy composite coating was greater than that of the pure epoxy coating.

The corrosion protection properties of β-CD-g-GO/epoxy coatings were studied by scratch testing at different exposure times, i.e., 0 and 84 h. The visible performances of the samples are presented in Fig. 13. The results clearly show the accumulation corrosion products around scratches on the steel sample with epoxy resin after 84 h. This is due to corrosion through the scribe to steel/coating interface. After the surface modification of steel substrates by β-CD-g-GO/epoxy composite coating, the amount of corrosion products formed near the scratches remarkably decreased. Hence, the β-CD-g-GO/epoxy

composite coating more effectively protected the steel substrate than did other coatings, as illustrated by EIS analysis.

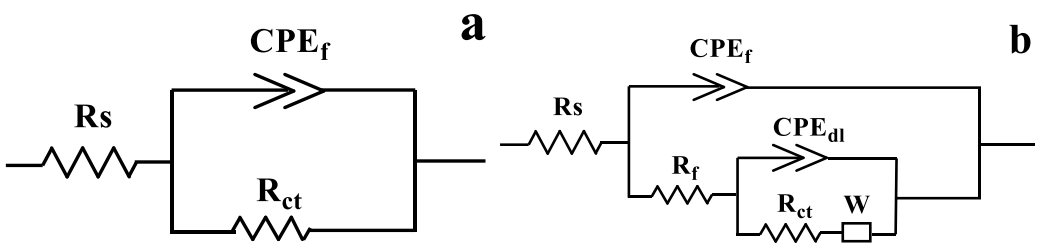

Figure 10. Equivalent circuit for the β-CD-g-GO/epoxy coating

Table 1. Fitting results of the equivalent electrical circuits after 2h immersion

coating	Pure epoxy	β-CD-g-GO/epoxy
Rc (Ω cm^2)	5.3556E8	2.2648E7
Rct(Ω cm^2)	3.2515E7	2.2161E7

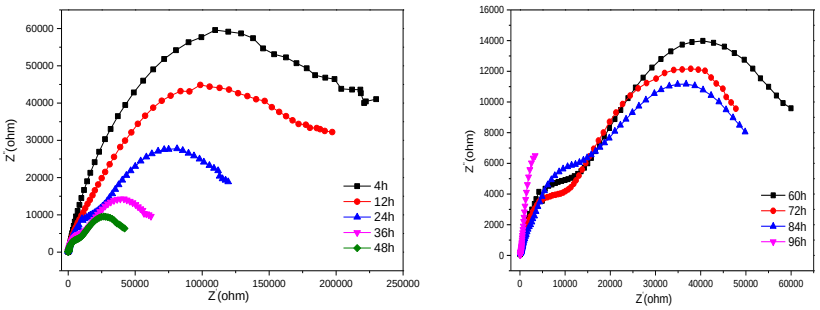

Figure 11. Impedance measurements of the pure epoxy coating from 4 h to 96 h

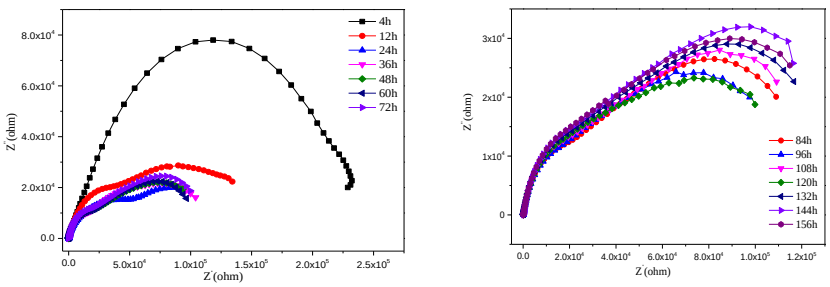

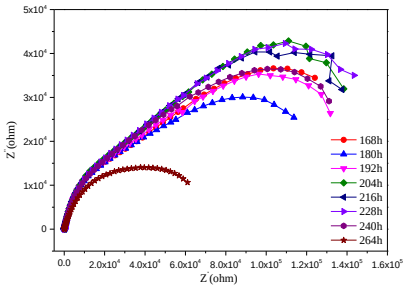

Figure 12. Impedance measurements of the β-CD-g-GO/epoxy coating from 4h to 264 h

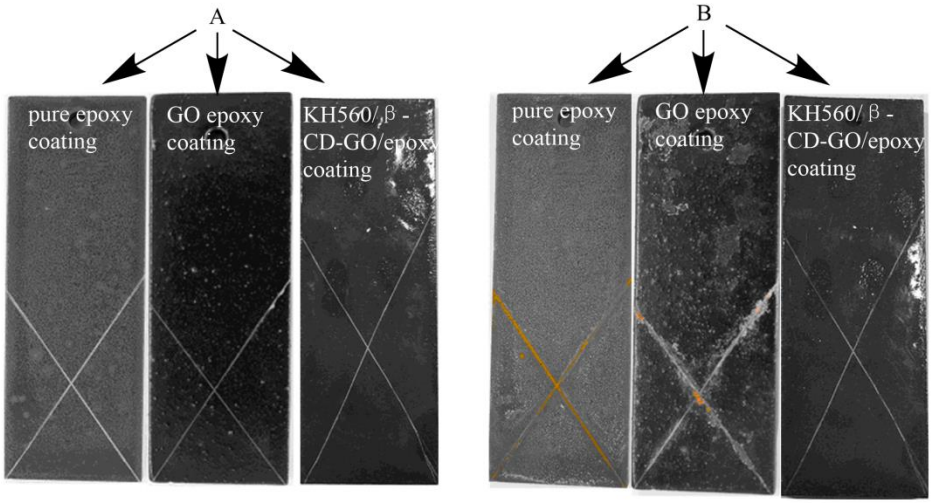

Figure 13. Visible performances of coatings exposed to NaCl solution for 0 (A) and 84 h (B)

4. CONCLUSIONS

β-CD-g-GO nanosheet materials were successfully synthesized via a simple and fast approach. In addition, the structure and morphology were characterized by FT-IR, XRD, TG and SEM. Afterward, the β-CD-g-GO/epoxy composition coatings was prepared by adding the β-CD-g-GO nanosheet materials to the epoxy resin. The β-CD-g-GO nanosheets were well-dispersed in epoxy matrix due to two dimensional sheet of Go. And the β-CD-g-GO/epoxy coating exhibited superior corrosion protection to the metals than pure epoxy coating.

ACKNOWLEDGEMENT
This work received the support of the Basic research and Strategic reserve Technology Fund of CNPC (2017Z-04), the National Natural Science Foundation of China (NO. 51804335), and the Open Fund (TLN201617) of State Key Laboratory of Oil and Gas Reservoir Geology and Exploitation (Southwest Petroleum University).

References

1. Z. Wang, E. Han, F. Liu, Z. Qian, L. Zhu, *J. Mater. Sci. Technol.*, 30 (2014) 1036.
2. H. Shi, F. Liu, E.H. Han, *J. Mater. Sci. Technol.*, 31 (2015) 512.

3. S. González, F. Cáceres, V. Fox, R.M. Souto, *Prog. Org. Coat*., 46 (2003) 317.
4. B. Ramezanzadeh, M. Khazaei, A. Rajabi, G. Heidari, D. Khazaei, *Corrosion -Houston Tx-*, 70 (2014) 56.
5. X. Shi, T.A. Nguyen, Z. Suo, Y. Liu, R. Avci, *Surface & Coatings Technology*, 204 (2009) 237.
6. I. Zaman, T.T. Phan, H.-C. Kuan, Q. Meng, L.T.B. La, L. Luong, O. Youssf, J. Ma, *Polymer*, 52 (2011) 1603.
7. J. Yu, R. Huo, C. Wu, X. Wu, G. Wang, P. Jiang, *Macromolecular research*, 20 (2012) 816.
8. X. Shi, T.A. Nguyen, Z. Suo, Y. Liu, R. Avci, *Surface and Coatings Technology*, 204 (2009) 237.
9. H. Feng, X. Wang, D. Wu, *Industrial & Engineering Chemistry Research*, 52 (2013) 10160.
10. S.K. Kumar, M. Castro, A. Saiter, L. Delbreilh, J.F. Feller, S. Thomas, Y. Grohens, *Materials Letters*, 96 (2013) 109.
11. M. Zabet, S. Moradian, Z. Ranjbar, N. Zanganeh, *Journal of Coatings Technology and Research*, 13 (2015) 191.
12. M.A. Soldatov, M.S. Parshina, V.V. Makarova, O.A. Serenko, A.M. Muzafarov, *Journal of Coatings Technology & Research*, (2017) 1.
13. M. Rajabi, G.R. Rashed, D. Zaarei, *Corrosion Engineering Science & Technology*, 50 (2014) 1743278214Y.000.
14. A. Ahmadi, B. Ramezanzadeh, M. Mahdavian, *Rsc Advances*, 6 (2016) 54102.
15. A.Y.H. Alhumade, *Express Polymer Letters*, 10 (2016) 1034.
16. L. Cavas, P.G. Yildiz, P. Mimigianni, A. Sapalidis, S. Nitodas, *Journal of Coatings Technology & Research*, (2017) 1.
17. S. Pourhashem, M.R. Vaezi, A. Rashidi, M.R. Bagherzadeh, *Progress in Organic Coatings*, 111 (2017) 47.
18. K.W. Putz, O.C. Compton, M.J. Palmeri, S.B.T. Nguyen, L.C. Brinson, *Advanced Functional Materials*, 20 (2010) 3322.
19. L.C. Tang, Y.J. Wan, D. Yan, Y.B. Pei, L. Zhao, Y.B. Li, L.B. Wu, J.X. Jiang, G.Q. Lai, *Carbon*, 60 (2013) 16.
20. Y. Ma, H. Di, Z. Yu, L. Liang, L. Liang, P. Yang, Y. Zhang, D. Yin, *Applied Surface Science*, 360 (2016) 936.
21. V.A. Mooss, A.A. Bhopale, P.P. Deshpande, A.A. Athawale, *Chemical Papers*, (2017) 1.
22. H. Zheng, Y. Shao, Y. Wang, G. Meng, B. Liu, *Corrosion Science*, (2017).
23. J.A. Shin, Y.G. Lim, K.H. Lee, *Journal of Organic Chemistry*, 77 (2012) 4117.
24. X. Liu, L. Meng, *Korean Journal of Chemical Engineering*, 30 (2013) 918.
25. J.W. Park, H.J. Song, *Journal of Physical Chemistry*, 93 (2002) 6454.
26. Y. Z, C. Q, L. L, P. Y, Z. G, H. Y, Water Sci Technol, 75 (2017) wst2017045.Z. Yu, L. Lv, Y. Ma, H. Di, Y. He, Rsc Advances, 6 (2016) 18217.
27. Z. Lin, Y. Yao, Z. Li, Y. Liu, Z. Li, C.P. Wong, *Journal of Physical Chemistry* C, 114 (2010) 14819.
28. I. Bratu, S. Astilean, C. Ionesc, E. Indrea, J.P. Huvenne, P. Legrand, *Spectrochimica Acta Part A Molecular & Biomolecular Spectroscopy*, 54 (1998) 191.
29. Y. Cao, J. Feng, P. Wu, *Carbon*, 48 (2010) 3834.
30. N. Yusoff, N.M. Huang, M.R. Muhamad, S.V. Kumar, H.N. Lim, I. Harrison, *Materials Letters*, 93 (2013) 393.
31. J. Szejtli, Cyclodextrins and their inclusion complexes, Akadaemiai Kiadao, 1982.
32. J. Chen, B. Yao, C. Li, G. Shi, *Carbon*, 64 (2013) 225.
33. K. Aasberg-Petersen, I. Dybkjær, C. Ovesen, N. Schjødt, J. Sehested, S. Thomsen, *Journal of Natural Gas Science and Engineering*, 3 (2011) 423.
34. X. Wang, S. Huang, L. Zhu, X. Tian, S. Li, H. Tang, *Carbon*, 69 (2014) 101.
35. Y.J. Wan, L.X. Gong, L.C. Tang, L.B. Wu, J.X. Jiang, *Composites Part A Applied Science & Manufacturing*, 64 (2014) 79.

36. Z. Yu, H. Di, Y. Ma, Y. He, L. Liang, L. Lv, X. Ran, Y. Pan, Z. Luo, *Surface & Coatings Technology,* 276 (2015) 471.
37. M. Nematollahi, M. Heidarian, M. Peikari, S.M. Kassiriha, N. Arianpouya, M. Esmaeilpour, *Corrosion Science*, 52 (2010) 1809.
38. Z. Yu, H. Di, Y. Ma, Y. He, L. Liang, L. Lv, X. Ran, Y. Pan, Z. Luo, *Surface and Coatings Technology*, 276 (2015) 471.
39. S. Qiu, C. Chen, M. Cui, W. Li, H. Zhao, L. Wang, *Applied Surface Science*, 407 (2017) 213.